Podosome rings generate forces that drive saltatory osteoclast migration

Shiqiong Hu[a,b], Emmanuelle Planus[c], Dan Georgess[d], Christophe Place[a,e], Xianghui Wang[b], Corinne Albiges-Rizo[c], Pierre Jurdic[d], and Jean-Christophe Géminard[a]

[a]Laboratoire de Physique, UMR 5672, Lyon 69364, France; [b]Department of Physics, State Key Laboratory of Precision Spectroscopy, East China Normal University, Shanghai 200062, China; [c]Institut Albert Bonniot, Université de Grenoble, Centre de Recherche INSERM-UJF U823, Equipe 1 DySAD–CNRS ERL 5284, Grenoble 38042, France; [d]Institut de Génomique Fonctionnelle de Lyon, Université de Lyon, UMS 3444 Biosciences, Gerland-Lyon Sud 69364, France; [e]Laboratoire Joliot-Curie, USR 3010, Ecole Normale Supérieure de Lyon, Centre National de la Recherche Scientifique, Lyon 69364, France

ABSTRACT **Podosomes are dynamic, actin-containing adhesion structures that collectively self-organize as rings. In this study, we first show by observing osteoclasts plated on bead-seeded soft substrates that podosome assemblies, such as rings, are involved in tension forces. During the expansion of a podosome ring, substrate displacement is oriented outward, suggesting that podosomal structures push the substrate away. To further elucidate the function of forces generated by podosomes, we analyze osteoclast migration. Determining the centers of mass of the whole cell (G) and of actin (P), we demonstrate that osteoclasts migrate by "jumps" and that the trajectories of G and P are strongly correlated. The velocity of the center of mass as a function of time reveals that osteoclasts rapidly catch up with podosomal structures in a periodic pattern. We conclude that actin dynamics inside the cell are not only correlated with cell migration, but drive it.**

Monitoring Editor
Alexander Mogilner
University of California, Davis

Received: Feb 1, 2011
Revised: Jun 24, 2011
Accepted: Jun 29, 2011

INTRODUCTION

Podosomes are structures, mainly made of actin, found in the contact region between cells and solid substrates. They consist of a dense, polymerized actin core surrounded by a "cloud," a loose, polymerized actin meshwork (Destaing *et al.*, 2003). Numerous proteins, such as actin regulators or focal adhesion proteins, are associated with these actin structures (Linder, 2009). Podosomes are typically formed in monocyte-derived cells (osteoclasts, macrophages, dendritic cells), endothelial cells, and smooth muscle cells. Studies of their molecular components have related them to invadopodia, which are mostly found in highly metastatic cancer cells. Even though there are some differences between these two actin-containing structures, they are very similar and are often referred to as *invadosomes* (Linder, 2009).

The main functions of invadosomes are considered to be cell adhesion and matrix degradation. They establish close contact with the substrate, and their formation requires integrins (Destaing *et al.*, 2010, 2011). Indeed, total internal reflection fluorescence (TIRF) microscopy has shown that podosomes are enriched in adhesion-mediating integrins and form only on the substrate-bound side of the cell (Linder and Aepfelbacher, 2003). Furthermore, there is increasing evidence that invadosomes are able to degrade extracellular matrix (Saltel *et al.*, 2008; West *et al.*, 2008; Linder, 2009). It recently has been proven that the invadosome-like structures of lymphocytes are involved in transcellular diapedesis, which has led to the suggestion that these structures could probe the endothelial cell surface to allow invasion (Carman *et al.*, 2007; Carman, 2009). Finally, podosomes are thought to play a role in cell migration and invasion by establishing localized anchorage, stabilizing sites of cell protrusion, and enabling directional movement (Linder and Kopp, 2005). However, there is no direct evidence proving the latter mechanism, and the role played by the podosomes in cell migration is still unknown.

This article was published online ahead of print in MBoC in Press (http://www.molbiolcell.org/cgi/doi/10.1091/mbc.E11-01-0086) on July 14, 2011.

Address correspondence to: Jean-Christophe Géminard (jean-christophe.geminard@ens-lyon.fr) or Pierre Jurdic (pierre-jurdic@ens-lyon.fr).

Abbreviations used: EDTA, ethylene diamine tetraacetic acid; FBS, fetal bovine serum; GFP, green fluorescent protein; M-CSF, macrophage colony–stimulating factor; αMEM, α-minimal essential medium; PBS, phosphate-buffered saline; PIV, particle image velocimetry; RANK-L, receptor activator of nuclear factor κB-ligand; SEM, scanning electron microscopy; TEMED, tetramethylethylenediamine; TIRF, total internal reflection fluorescence.

Osteoclasts, the bone-resorbing cells, are large, multinucleated hematopoietic cells that exhibit podosomes when adherent, for instance, on plastic or glass. We have previously shown that podosomes can collectively self-assemble in osteoclasts. They can aggregate in clusters that later form rings. In a transient regime, the rings grow before they dissociate. Podosome rings eventually end up forming belts at the periphery of mature osteoclasts at rest. These belts require an intact microtubule network (Destaing *et al.*, 2003, 2005), contrary to clusters and rings that are microtubule-independent. When adherent on a mineralized extracellular matrix, osteoclasts polarize and podosomes condense to form a large sealing zone delineating the resorption area (Luxenburg *et al.*, 2007; Saltel *et al.*, 2011). This dynamic patterning of podosomes in osteoclasts recently has been shown to depend on the topography of the substrate (Geblinger *et al.*, 2010). These latter data correlate well with previously described results that provided the first evidence that invadosomes in rosettes, found in either NIH3T3 fibroblasts or src-transformed BHK cells, are major sites through which cells sense mechanical forces and exert traction forces (Collin *et al.*, 2006, 2008). Nonetheless, the molecular mechanisms governing these forces remain unknown (Destaing *et al.*, 2003; Saltel *et al.*, 2004).

In this study, we describe a series of experiments designed to elucidate the role played by podosomes in the spreading, migration, and retraction of osteoclasts. At one end of the spectrum, we report observations of actin structures at a short time scale: we describe the spatial organization of podosomes during early adhesion and retraction. We also report the evolution of the three-dimensional shape of an osteoclast in relation to the organization of podosomes in the contact region between the cell membrane and the substrate. We also qualitatively characterize the force applied by the osteoclast onto the substrate. At the other end of the spectrum, we report a study of the migration process of a single osteoclast at a long time scale, and investigate how the motion of the cell is related to the collective organization of actin. The whole set of experimental results makes it possible to discuss the role of the podosomal structures in osteoclast motility and adhesion processes.

RESULTS

Podosomes are involved in maintaining tension in osteoclasts

To further characterize the role of podosomes in osteoclast adhesion, we first observed their behavior during spreading and, inversely, detachment. We used a RAW macrophage cell line stably expressing actin fused to GFP (Destaing *et al.*, 2003) and differentiating into osteoclasts in presence of the two cytokines macrophage colony–stimulating factor (M-CSF) and receptor activator of nuclear factor κB-ligand (RANK-L). In our first experiment, we observed the dynamics of the GFP-actin during the early adhesion process: mature osteoclasts were detached and then seeded on glass. The experiment consisted of observing the attachment and spreading by Normarski contrast and fluorescence time-lapse microscopy (Figure 1A and Supplemental Movie 1). We observed that the osteoclast, which was initially round before adhering, rapidly spread by forming membrane protrusions, reminiscent of corollas, around the central part of the cell. Simultaneously, GFP-actin, which was initially scattered throughout the cell, concentrated at the periphery of the spreading areas and started forming clearly recognizable podosomes marked by dense actin cores within 12 min of seeding. Additional immunofluorescence staining of actin and vinculin, a podosome cloud component, confirmed the osteoclast is adherent but does not make podosomes during the first 10 min after seeding; actin is loosely distributed in the cytoplasm and vinculin localizes at the periphery of the cell but does not participate in any organized structures. However, when the osteoclast starts spreading, typical podosomes with F-actin cores and vinculin-containing clouds start to form (Figure 1B). These observations revealed that a reorganization of actin results from or drives the spreading process. In a second experiment, adherent osteoclasts were slowly detached by ethylene diamine tetraacetic acid (EDTA) treatment. We observed that membrane retraction occurred right after the disappearance of podosomes (Figure 1C and Supplemental Movie 2). Indeed, within 2 min of EDTA treatment, all the podosomes dismantled, whereas osteoclasts retracted slowly but remained adherent. From these observations, we concluded podosomes are not strictly necessary

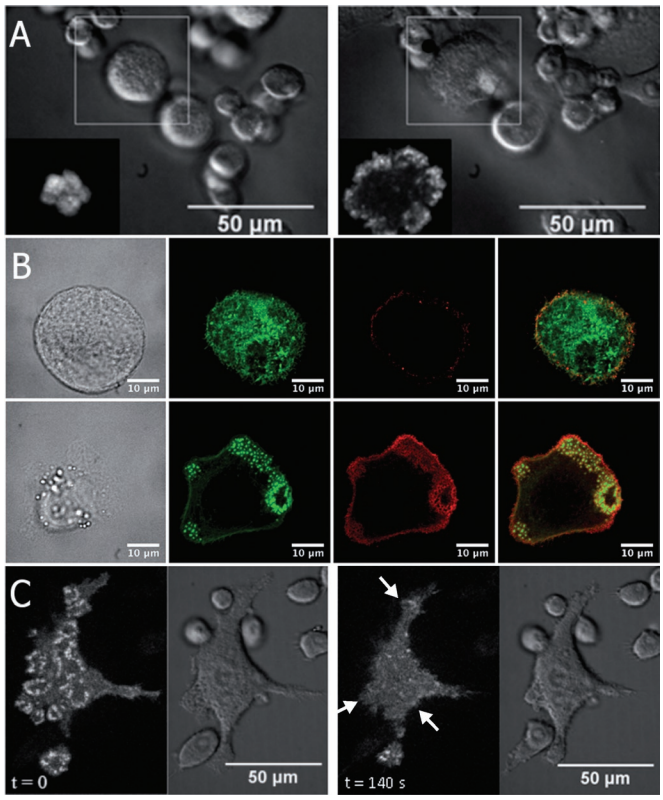

FIGURE 1: Podosomes are involved in maintaining tension in osteoclasts. (A) During adhesion and spreading processes, the podosomes accumulate along the periphery of the cell, in the expanding regions. Several mature osteoclasts expressing GFP-actin are seeded onto a glass coverslip and observed under the microscope using a Nomarski contrast. Insets, fluorescence image of the cell, which is indicated by the white square. Left, 5 min after seeding, the cell is round and actin is scattered in the cytoplasm (inset). Right, 20 min after seeding, the considered cell starts spreading. The fluorescence image (inset) reveals that actin becomes concentrated in podosomes along the periphery of the contact region, where the cell is expanding. (B) Immunofluorescence labeling of adherent osteoclasts spreading on glass: actin stained with phalloidin (green) and vinculin stained with anti-vinculin (red). Top, 10 min after seeding, actin is loosely distributed in the cytoplasm of the osteoclast and vinculin staining confirms the absence of podosomes. Bottom, 25 min after seeding, podosomes form where the cell is expanding. Vinculin marks the periphery (surrounding cloud) of the podosomes. (C) Osteoclasts remain adherent even in the absence of podosomes. At t = 0 s, the cell is spread, in close contact with the substrate (right), and the fluorescence image (left) reveals several rings of podosomes (bright spots). At t = 40 s, the addition of EDTA produces a rapid dissociation of podosomes associated with cell retraction (white arrows).

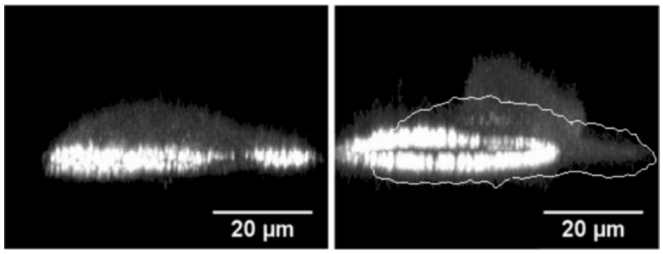

FIGURE 2: The podosome ring expansion correlates with the direction of migration. One osteoclast expressing the GFP-actin adherent on glass is imaged under the confocal microscope. The actin organization in the contact area with the substrate is revealed by slightly tilting the reconstructed images along the *z*-axis. Left, actin, concentrated in the base plane, is organized in two rings, with the largest ring located on the left-hand side. The fluorescence signal from the actin monomers ubiquitously invading the cytoplasm clearly reveals the shape of the cell. Right, 75 min later, the largest ring grows and the smallest disappears. Simultaneously, the cell flattens above the remaining ring, expanding in that region, and also moving to the left (white contour corresponds to the initial shape of the cell shown on the left).

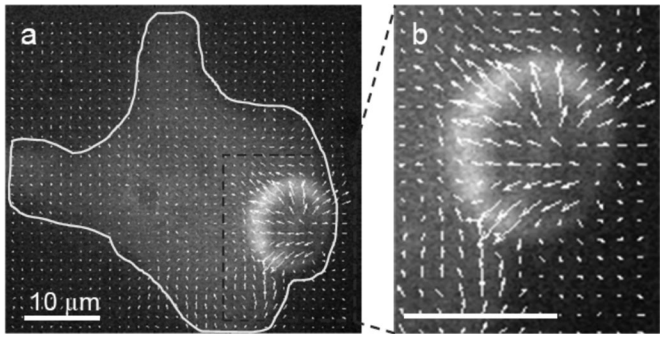

FIGURE 3: Actin ring structures exert tension forces on the substrate. The dynamics of a live osteoclast, expressing GFP-actin moving on the surface of a soft polyacrylamide gel (stiffness: 0.5 kPa) are shown. The gel containing fluorescent beads (rhodamine, diameter 210 nm) is coated with vitronectin. Images of GFP-actin and of the rhodamine beads were taken every minute. The substrate displacement field is reconstructed by tracking the displacements of the fluorescent beads. (A) The merge of the osteoclast image (GFP-actin) and of the displacement field (arrows indicate the local displacement with respect to the substrate at rest) reveals displacement is significant solely around the podosomal structure (ring). (B) Enlargement of the podosomal structure as delineated by the rectangle in (A). The displacements of the beads clearly reveal that the ring pushes the substrate outward.

for osteoclast adhesion but rather play a role in exerting tension needed for spreading.

The expansion of a podosome ring induces cell displacement

To further determine the interaction between actin dynamics and osteoclast migratory behavior, we assessed the three-dimensional shape of an osteoclast vis-à-vis the organization of actin in the contact region between the cell and the substrate. As an osteoclast migrated on a glass dish, we used confocal time-lapse microscopy to image *z*-planes every 15 min. Then Z-stacks were used to reconstruct the three-dimensional shape of the cell based on a fluorescence signal from G-actin diffusing ubiquitously in the cytoplasm (Figure 2 and Supplemental Movie 3). These observations revealed that the growth of a podosome ring in the contact region is associated with a rapid flattening and migration of the cell. Again, the dynamics of the actin structure inside the cell were proven to be strongly correlated with the spreading and migration processes.

Podosome structures exert tension on the substrate

To assess the forces exerted by an adherent osteoclast, we observed the deformation of the substrate induced by the cell. To do so, we used a soft polyacrylamide gel (stiffness: 0.5 kPa) coated with vitronectin to allow adhesion (Figure 3). The experiment revealed that the displacement of the fluorescent beads in the gel is concentrated around the podosome ring, whereas no displacement was ever observed in the regions devoid of podosomes (Figure 3A). Furthermore, when the podosome ring grew and spread, the substrate displacement was mainly oriented outward from the ring (Figure 3B, white arrows). Thus the podosome ring is subjected to an internal tension that tends to increase its perimeter and extend the ring toward the periphery (negative tension). As a consequence, the substrate exerts a compressive force and tends to reduce the size of the ring. To conclude, the podosome ring is clearly associated with a tensional effect that stretches the cellular membrane.

Podosome ring expansion drives osteoclast migration

To comprehend the role played by podosome rings in cell motility, we observed the motion of several mature osteoclasts expressing GFP-actin, seeded on a vitronectin-coated soft polyacrylamide gel (stiffness: 3 kPa). (We chose to work with the same substrate as the one used for the force measurement to obtain a complete set of experiments under similar conditions). Images were obtained using time-lapse microscopy every 5 min for ~8 h (Figure 4 and Supplemental Movie 4). Qualitatively, in the whole set of experiments (four mature osteoclasts on polyacrylamide gel), we observed that the cell migrates randomly. More precisely, the formation of podosome rings inside the osteoclast accompanies its elongation in one given direction. When the maximal length (L) of the cell is about twice its typical size, the actin structure disappears from one side, and the cell retracts toward the remaining structure on the opposite side, which becomes the leading edge (Figure 4; t = 120 min). This results in a "jump" of the cell in the corresponding direction (Figure 4; t = 150–180 min). Subsequently, the cell elongates in an almost perpendicular direction due to the growth of two new rings from the remaining structure at the leading edge (Figure 4; t = 120 min). In the following paragraphs, we report a representative quantitative study of the cell motion.

First, we focused on the dynamics of the cell's center of mass, G (see *Materials and Methods*). We reported the trajectory of G in the sample plane (*x*, *y*) during the whole experimental time (Figures 4, Bottom, right, and 5). The first striking result is that the cell moves in a series of straight jumps separated by spatially localized changes in direction. To get information about the dynamics, we reported the velocity of the center of mass, V_G, as a function of time, t (Figure 6A), and noticed V_G exhibits large peaks (A to D) almost periodically every 2 h.

Then, in order to account for the potential coupling between the motility of the cell, characterized by the motion of the center of mass G, and the internal dynamics of actin, we defined a point, P, summarizing the position of all actin inside the cell (see *Materials and Methods*). We also defined the vector $\vec{f} \equiv \overrightarrow{GP}$, which accounts for the distance and direction between the center of mass G and the location of actin P (Figure 4). Reporting the trajectory of P in the (*x*, *y*) plane (Figure 5), we observed first that G and P experience the same trajectories. To provide information about the dynamics, we

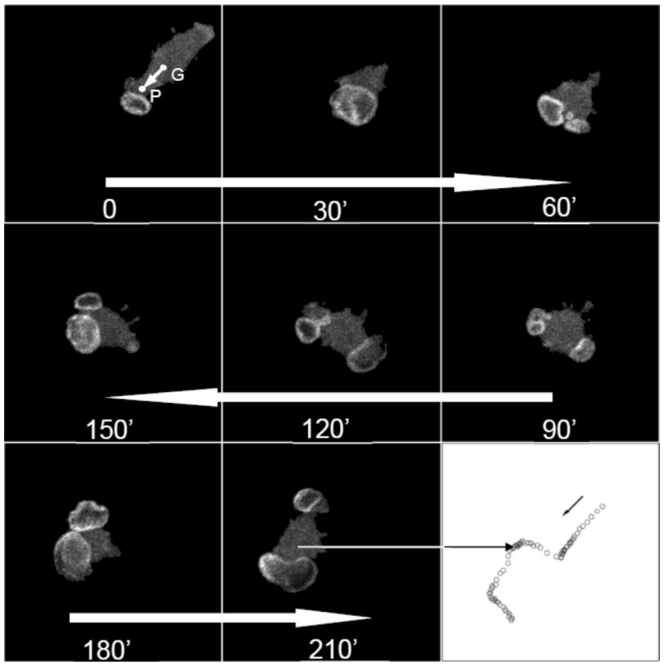

FIGURE 4: Podosome ring expansion and osteoclast migration are correlated. The dynamics of an osteoclast expressing GFP-actin moving on the surface of a polyacrylamide gel (stiffness: 3 kPa) are shown using time-lapse fluorescence microscopy (Supplemental Movie 4). Eight successive images separated by 30 min are displayed. The center of mass of the cell G, the position of the actin structure P, and defined the vector $\vec{f} \equiv \overrightarrow{GP}$ were determined from such images (see *Materials and Methods*). The points G and P for the first image (t = 0, top, left) are indicated. Bottom, right, successive positions, separated by 5 min, of the center of mass G determined from this image sequence (same scale).

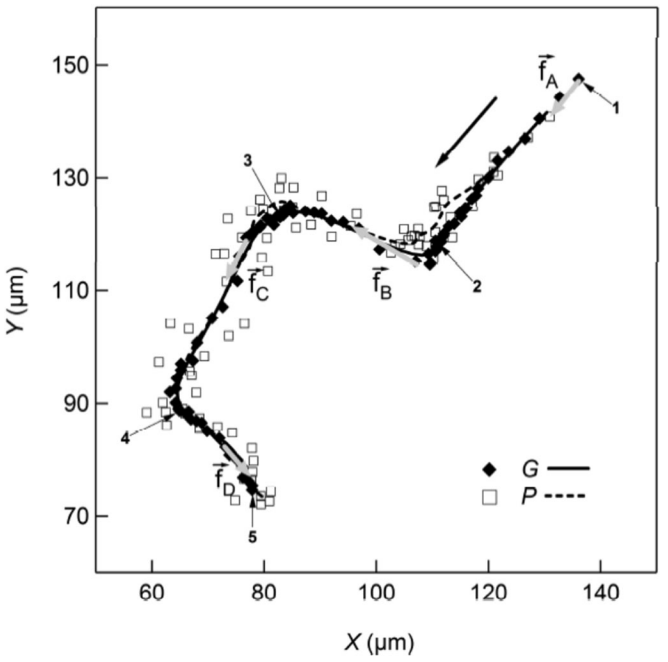

FIGURE 5: Successive positions of the center of mass G and of actin P in the sample plane (*x, y*). The time difference between two successive points is 5 min. The black arrow indicates the direction of the motion. The continuous and dashed lines correspond to the trajectory of G and P, respectively, averaged over 10 successive positions. The trajectories of G (full diamonds) and P (open squares) are strongly correlated. The vectors $\vec{f}_A$, $\vec{f}_B$, $\vec{f}_C$ and $\vec{f}_D$ (gray arrows) are associated to the events A, B, C, and D, and labels 1–5 indicate the minima in the velocity V_G, as defined in Figure 6.

reported the distance $\vec{f} \equiv \|\overrightarrow{GP}\|$ between G and P as a function of time t (Figure 6B). We then observed that f and V_G are also strongly correlated in time, a large peak in f preceding each large peak in V_G. The temporal correlation between f and V_G, and especially the delay τ between the peak in f and the peak in V_G, can be assessed by calculating the cross-correlation function $\chi(t) \equiv \int f(t' - t)\, V_G(t')dt$, where the integral is estimated over the whole experimental time (Figure 7). The experimental correlation function $\chi(t)$ exhibited a maximum for $t \equiv \tau \approx 10$ min, whereas the oscillations pointed out the period of the cell motion, $T \approx 2$ h. In the same way, we reported the cell length L as a function of time t (Figure 6C). We observed that the cell length L increased almost linearly between two successive jumps. The disappearance of one of the actin structures on one side leads to a peak in f when L is maximum (Figure 6B).

We considered the direction of the jumps by identifying first the peaks A, B, C, and D, as defined in Figure 6, and the associated minima in the velocity (numbered from 1 to 5, such that peak A is associated with the jump from G_1 to G_2, etc.). We denoted $\vec{f}_A$, $\vec{f}_B$, $\vec{f}_C$, and $\vec{f}_D$, the values of $\vec{f}$ at the peaks A, B, C, and D, and $\overrightarrow{\Delta G_{ij}} \equiv \overrightarrow{G_i G_j}$, the vector associated to the displacement of G during the jumps from i to j. Reporting the values of $\vec{f}$ at the maxima and the corresponding displacements $\overrightarrow{\Delta G}$, we observed that these quantities are correlated in both length and direction (Figure 8). First, the angles θ_P and θ_G that $\vec{f}$ and $\overrightarrow{\Delta G}$ make with the *x*-axis are equal (Figure 8A), which proves the jumps occur in the direction of $\vec{f}$. Second, the amplitude $\overrightarrow{\Delta G}$ of the jumps is proportional to f (or, equivalently, to L; Figure 8B). Finally, note that successive jumps occur in directions making angles of ~90 degrees between them (Figure 8).

As a conclusion of this last experiment, the osteoclast jumps follow the internal organization of actin. We maintain that the point P refers to all G-actin monomers in the cell, including the ones present in structures made of F-actin polymers. We show that the growth of rings induces the elongation of the cell. When the length L of the cell in a given direction is about twice its initial size before expansion, one of the actin rings takes the lead at one end, whereas the others disassemble. Subsequently, the cell retracts toward the remaining structures, which leads to a jump of the cell in the given direction ~10 min after f (or L) has reached a maximum. The process repeats itself almost periodically every 2 h. Thus the motion of the cell occurs by seemingly periodic jumps, the length of each jump correlating to the cell's length, during which the cell moves rapidly in a given direction, resulting in saltatory migration.

DISCUSSION

We have investigated the role played by podosomes in the migratory behavior of osteoclasts. In summary, podosome rings exert tension forces that tend to extend the cellular membrane and push the substrate outward. Podosome assemblies, even in close contact with the substrate, do not play a direct role in cell adhesion; rather, they exert forces where tension is needed, forming in expanding regions and disappearing from retracting regions. Discussing in detail the migration of a set of osteoclasts from a RAW monocytic cell line expressing an actin green fluorescent protein (GFP), we showed that osteoclasts move by jumps, rapidly catching up with podosomal structures in a periodic pattern.

We wish to emphasize that our experimental observations are not too specific and do correspond to a general pattern. First, we can state that all the RAW-derived osteoclasts we observed were

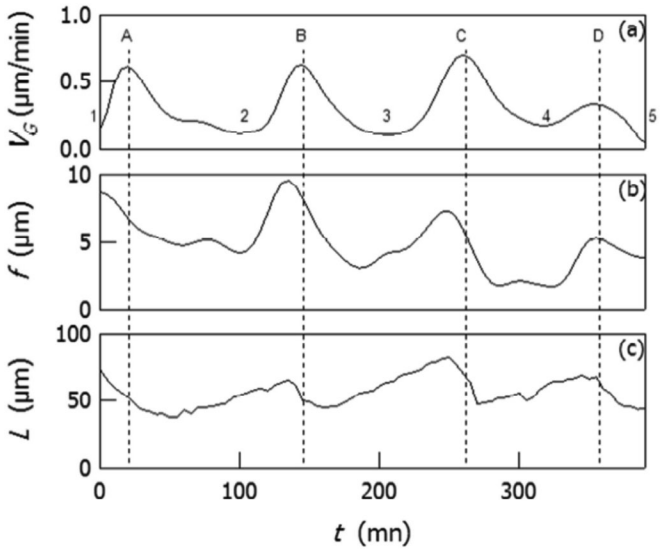

FIGURE 6: Velocity of the center of mass V_G, distance f, and cell length L as a function of time t. (A) The velocity V_G exhibits peaks, which correspond to a rapid motion of the cell in a given direction (jump). The minima in the velocity V_G are labeled 1–5. (B) The distance f interestingly exhibits the same type of temporal evolution. (C) The cell length L increases slowly when the cell velocity is small, and rapidly decreases during the jumps. Note that the cell jumps ~10 min after f or L have reached a maximum. Identified here are four events: A, B, C, and D. Successive jumps are separated by ~2 h.

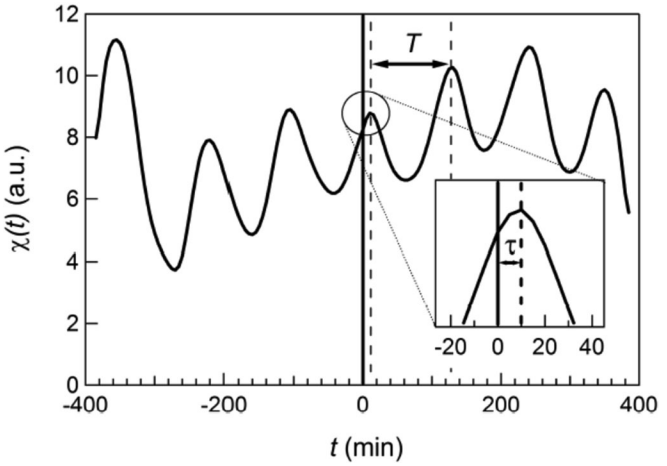

FIGURE 7: Temporal cross-correlation (t) between the distance f and the cell velocity V_G. The oscillations of the correlation function confirm the almost periodic character of the jumps, with a period T ≈ 2 h. Inset, enlargement of the central peak. The correlation (t) is maximum for t ≡ τ ≈ 10 min, which shows that the cell jumps ~10 min after f has reached a maximum.

exhibiting qualitatively the same type of motion as proven by cells exhibiting mainly two or more podosome rings, and even podosome clusters (Supplemental Movie 5). Second, in order to confirm results with different substrate and osteoclast origins, we also studied the dynamics of primary osteoclasts expressing LifeAct-eGFP moving on glass. We observed the exact same migration pattern (Supplemental Data 6 and Supplemental Movie 6). These experiments demonstrate that the observed pattern is not specific to the RAW cell line and substrate (vitronectin-coated polyacrylamide) and that the dynamics of actin inside the osteoclast are not only correlated with cell migration, but drive it.

We propose a potential mechanism that accounts for osteoclast migration. The migration of osteoclasts involves their elongation, which is correlated with the growth of podosome rings. Podosomes collectively push the cell membrane outward, as already observed during the early spreading process. From the observation of substrate displacement, we concluded, in agreement with previous investigations on BHK-RSV cells showing torsional tractions underneath the podosome rings (Collin *et al.*, 2008), that podosome rings exert forces onto the substrate. We propose that the associated substrate displacement, which points outward, subjects the ring to an internal tension that tends to extend the ring. Thus the formation and growth of a podosome ring can account for the spreading of the contact region. Indeed, a podosome ring that encounters the cell periphery pushes the membrane outward. The process can take place until the membrane has reached its maximum possible extension (the cell is then flat). If two rings are pushing the cell in opposite directions, the cell length increases until the weakest ring loses its mechanical stability because of excessive stress. Then the weaker disappears and the cell jumps in the direction of the remaining ring.

Finally, we discuss the physical origin of the tension force. Individual podosomes are associated with a dense actin core formed by cross-linked actin filaments, as demonstrated by scanning electron microscopy (SEM) observation experiments (Luxenburg *et al.*, 2007).

We have previously proposed that actin cores have a conical shape (Destaing *et al.*, 2003; Jurdic *et al.*, 2006; Hu *et al.*, 2011); they are dynamical structures growing from the cell membrane at the substrate interface and dissociating from the top (Figure 9A). Considering the sketch in the Figure 9B, one can easily see that, because of a steric frustration effect, the base of the cone tends to extend if the structure grows from the base and the filaments are linked to one another. As a consequence, two neighboring podosomes tend to repel each other, which naturally explains why a ring structure is subjected to an internal tension that tends to increase the length of a podosome line (negative tension) and, accordingly, the ring diameter. In such a scenario, the podosomes are responsible for the membrane tension. What remains unexplained are the molecular mechanisms involved in the transmission of tension from the membrane to the substrate at the podosome base.

The mechanism we propose is based on several assumptions (for instance, the cell adheres to the substrate in the contact region and the podosomal structure becomes unstable when the stress is

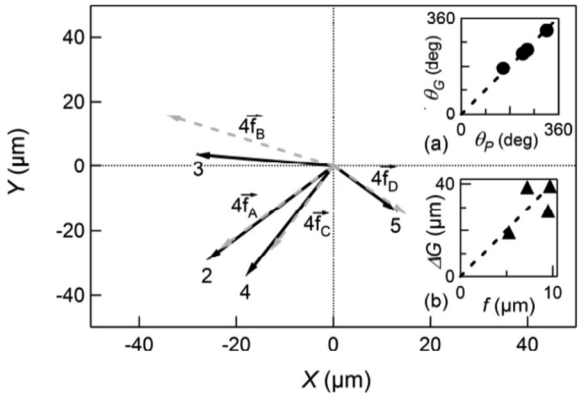

FIGURE 8: Vectors $\vec{f}_A, \vec{f}_B, \vec{f}_C$ and associated displacements $\overline{\Delta G}$. The cell center of mass G jumps toward P, as pointed out by the strong correlation between at the maximum (gray dotted arrows) and the corresponding $\overline{\Delta G}$ (black arrows). (A) Angle θ_G vs. angle θ_P. The dotted line corresponds to the slope 1, showing that $\theta_G \approx \theta_P$. (B) Jump length $\overline{\Delta G}$ vs. maximum distance f. The cell moves over a larger distance when the distance f at the maximum is larger.

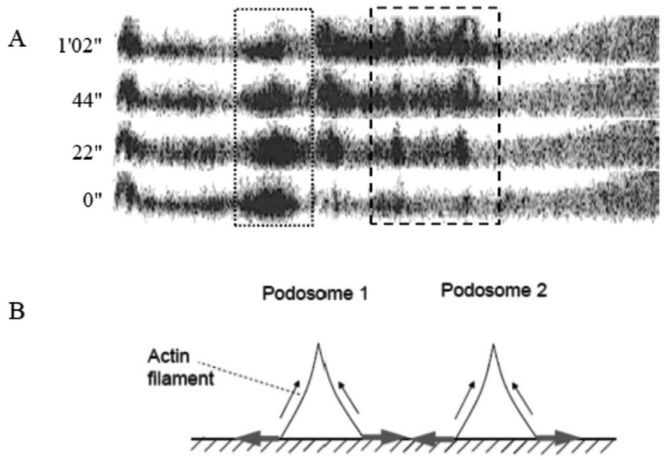

FIGURE 9: Sketch of forces exerted by two growing podosomes. (A) Podosomes in the contact region between an osteoclast and a glass bottom dish were imaged under the confocal microscope. Stacks of pictures were then used to reconstitute a Z-image, rendering the profiles of the podosomes in a vertical plane (t = 0, 22, 44, and 62 s). The sequence shows that the podosomes consists of actin filaments growing rapidly from the cell membrane (thick dotted rectangle on the right) and disappearing from the top (dotted rectangle on the left). (B) We have previously proposed that the actin cores of podosomes are organized in a conical brush (Destaing *et al.*, 2003; Jurdic *et al.*, 2006, Hu *et al.*, 2011). Because actin filaments are cross-linked and growing from the membrane, the actin filaments, due to steric constraints, repel each other in the base plane. Thus two neighboring podosomes tend naturally to repel each other, and generate the negative tension associated with the podosomal structure. Gray arrows, forces exerted by neighboring podosomes on the substrate.

released), but it is compatible with the seemingly periodic movement of the cell in the direction of $\overrightarrow{GP}$, thus toward the actin structure. First, as explained above, the cell moves in the direction of $\overrightarrow{GP}$. One can estimate the growth velocity of the ring from the period T, which corresponds to the time needed for two rings to push the cell membrane over a distance that compares to the cell size. From the slope $\frac{dL}{dt}$ (Figure 6C), we have estimated that the ring growth velocity is on the order of $v \approx 0.25$ µm/min (L increases by ~50 µm in 100 min due to the action of two rings). From the growth velocity v, taking into account the typical distance between two podosomes (~1 µm), we estimate the typical lifespan of one podosome is ~4 min. The latter estimate agrees reasonably with previous results (Destaing *et al.*, 2003; Geblinger *et al.*, 2010), which again sustains our model. Second, it is interesting to note that the assumption that the podosomal structure becomes unstable when the stress is released would be compatible with the fact that successive jumps make a 90-degree angle between them, at least when two rings develop in opposite directions. Indeed, when the cell reaches its maximum elongation, the disappearance of one of the podosomal structures releases the stress along $\vec{f}$. As a consequence, the remaining podosomal structure becomes unstable along $\vec{f}$. This instability could explain why two secondary rings, aligned in a perpendicular direction, form and grow from the remaining ring.

The saltatory migration of osteoclasts described here is reminiscent of the saltatory migration of oligodendrocyte precursors dispersing from the ventricular zone during early brain development and described as existing in alternating stationary and fast-moving phases (Tsai *et al.*, 2009). It could reflect the inchworm-like progression of bone-resorbing osteoclasts we described earlier (Saltel *et al.*, 2004).

MATERIALS AND METHODS

Osteoclast differentiation

To image podosomes in osteoclasts, we have used the RAW monocytic cell line expressing an actin GFP (Destaing *et al.*, 2003). The RAW 264.7 cells, from the American Type Culture Collection (Manassas, VA), were transfected in our lab with FuGENE 6 following manufacturer's recommendations (Roche Diagnostics, Indianapolis, IN). The cells then were regularly selected by flow cytometry (FACScan, Becton Dickinson, San Jose, CA) to maintain a stable RAW cell line expressing GFP-actin. The GFP-actin RAW cells were cultured with a density of ~50 cells/mm^2 in a 12-well plate for 6 d, which is the optimum time for differentiation into osteoclasts. Primary murine osteoclasts were differentiated from the bone marrow of 8-wk-old mice, as described in Destaing *et al.* (2003). The differentiation medium was α-minimal essential medium (αMEM; Invitrogen, Carlsbad, CA) containing 10% fetal bovine serum (FBS; Biowest, Nuaillé, France), 30 ng/ml M-CSF, and 35 ng/ml RANK-L. Recombinant human RANK-L and human M-CSF were produced in our laboratory as previously described (Destaing *et al.*, 2003). Culture medium was changed every 2 d. After 6 d of differentiation, mature osteoclasts were washed twice with phosphate-buffered saline (PBS; Invitrogen) and detached by using 0.25 µM EDTA (Invitrogen) in PBS for 5 min (EDTA chelates divalent ions essential for activating membrane receptors involved in cell adhesion). After centrifugation, osteoclasts were seeded with a density of ~100 cells/mm^2, either on a glass bottom dish (MatTeK, Ashland, MA) or on a polyacrylamide gel.

Transient transfection

For video microscopy of the actin cytoskeleton in primary osteoclasts, day 4 osteoclasts were transfected with pEGFP-N1-LifeAct (Riedl *et al.*, 2008) using Lipofectamine LTX with PLUS Reagent (Invitrogen) following the manufacturer's instructions. After 48 h, cells were detached using EDTA, and replated on a glass bottom dish, as described in the preceding section.

Indirect immunofluorescence

To observe podosome formation during spreading, we reseeded osteoclasts derived from RAW 264.7 cells on a glass bottom dish as previously described. Briefly, cells were fixed with 4% paraformaldehyde (pH 7.2) at 10 min and 25 min after reseeding. They were permeabilized with 0.2% Triton-X-100 in PBS, and then incubated for 1 h with anti-Vinculin antibody (Clone hVIN1, #V9264; Sigma-Aldrich, St. Louis, MO) at 10 µg/ml final concentration. Cells were then washed three times with PBS and incubated with Alexa Fluor 488 phalloidin (Life Technologies) and Alexa Fluor 647 goat anti–mouse immunoglobulin G (A21236; Life Technologies) at 2 µg/ml for 45 min. Samples were washed and kept in PBS for microscopy.

Confocal microscopy

Living cells were imaged in an inverted microscope (DMI 4000; Leica) equipped with a confocal spinning-disk unit (CUS22; Yokogawa, Tokyo, Japan) and an incubating chamber at 37°C with 5% CO_2 and humidity-saturated atmosphere. The light source consisted of a laser diode (excitation wavelength 491 and 647 nm; Roper Scientific) and an emission filter with a 500- to 550-nm or 641- to 708-nm bandpass (Semrock, Lake Forest, IL). For time-lapse microscopy, we recorded, during 8 h, one image from a QuantEM camera (Photometric, Tucson, AZ) every 5 min using a 20× objective. For fixed samples, we used a 100× oil immersion objective.

Soft-gel substrate

Polyacrylamide gels were prepared at the bottom surface (14-mm diameter) of glass bottom dishes (MatTeK). First, the glass bottom surfaces of the MatTek culture dishes were pretreated with 500 µl Bind-Silane (g-methacryloxypropyltrimethoxysilane; GE Healthcare, Waukesha, WI) by applying the solution with a cotton swab and then drying the surface under a hood. At the same time, glass coverslips (12-mm diameter) were quickly treated with 15 µl Sigmacote (Sigma) and then dried under the hood.

Polyacrylamide gels exhibiting two different rigidities were obtained, according to the ratio 8% acrylamide/0.05% bis-acrylamide for a very soft gel (stiffness: 0.5 kPa) or the ratio 8% acrylamide/0.1% bis-acrylamide for a soft gel (stiffness: 3 kPa). Fluorescent beads (210-nm diameter; Molecular Probes, Invitrogen) were seeded in the softer gel. A 2.5 ml solution was obtained by mixing 500 µl acrylamide 40%, 62.5 µl bis-acrylamide 2%, 25 µl HEPES (1M, pH 8.5), 80 µl 2% bead solution, and water. Then 12.5 µl ammonium persulfate and 1.25 µl tetramethylethylenediamine (TEMED) were added to allow polymerization. The final solution (8 µl) was dropped on a Bind-Silane–treated MatTek dish coverslip, which was then covered by a Sigmacote-treated coverslip. After 20 min of polymerization, the upper coverslip was removed.

Finally, the gel surface was activated with vitronectin (BD Biosciences; Damljanovic *et al.*, 2005). Briefly, pure hydrazine hydrate (Sigma) was added to the gels for 2 h; the gels were then washed first with 5% glacial acetic acid for 1 h and then with distilled water for 1 h. Vitronectin solution (10 µg/ml) was diluted in 50 mM sodium acetate buffer at pH 4. The oxidation of vitronectin was achieved by adding 3.6 mg/ml sodium periodate crystals (Sigma) and incubating the gels at room temperature for 30 min. Oxidized vitronectin (150 µl) was added on the polyacrylamide-treated gel, which was incubated at room temperature for 1 h and then washed with PBS.

Analysis of the substrate displacement field

We used the open software package JPIV for particle image velocimetry (PIV; www.jpiv.vennemann-online.de) to determine the displacements of the fluorescent beads in the (*x*, *y*) plane with respect to their initial positions.

Cell-tracking image analysis

Stacks of images and associated data were analyzed using the image processing and analysis software ImageJ (Abramoff *et al.*, 2004) and the technical graphing and data analysis software Igor Pro (WaveMetrics, Lake Oswego, OR). We denoted M and N the dimensions in pixels of the image in the directions m and n, respectively. We determined the position (m_G, n_G) of the center of mass of a cell, G.

From one raw fluorescence image I_{mn}, using an intensity threshold, we obtained a binary image B_{mn} of the cell such that $B_{mn} = 1$ if the indices m and n correspond to a point inside the cell and $B_{mn} = 0$ otherwise. By definition, $m_G \equiv \frac{1}{NM}\sum_{n=1}^{N}\sum_{m=1}^{N} mB_{mn}$ and $n_G \equiv \frac{1}{NM}\sum_{n=1}^{N}\sum_{m=1}^{N} nB_{mn}$ are the position (m_P, n_P) of actin, P.

To obtain a point P, which characterizes the position of actin inside the cell, from one raw fluorescence image, we defined $m_P \equiv \frac{1}{NM}\sum_{n=1}^{N}\sum_{m=1}^{N} mI_{mn}^{\alpha}$, and $n_P \equiv \frac{1}{NM}\sum_{n=1}^{N}\sum_{m=1}^{N} mI_{mn}^{\alpha}$. We introduced the exponent α in order to increase the contrast. We checked that the experimental results did not depend significantly on α, and report results obtained with $\alpha = 3$.

Finally, scaling factors were applied to convert (m_G, n_G) and (m_P, n_P) to the positions (x_G, y_G) and (x_P, y_P) in the sample plane (*x*, *y*).

ACKNOWLEDGMENTS

We thank C. Chamot and C. Lyonnet from the Imaging Platform (PLATIM) of UMS3444/US8 Biosciences, Lyon, France, for their help and advice; C. Domenget and all members of P. Jurdic's team for their support and assistance in osteoclast cultures; and O. Destaing (Institut Albert Bonniot, Université de Grenoble, Centre de Recherche INSERM-UJF U823, Equipe 1 DySAD—Centre National de la Recherche Scientifique ERL 5284, Grenoble, France) and F. Saltel (Institut Européen de Chimie-Biologie, Université de Bordeaux, Pessac, France & INSERM Unité 889, Bordeaux, France) for Figure 9A. This work was supported by recurrent grants from Centre National de la Recherche Scientifique and Ecole Normale Supérieure de Lyon and grants from the Association pour la Recherche sur le Cancer (ARC), the Agence Nationale de la Recherche ("ANR-podosomes"), and the Fondation pour la Recherche Médicale (DEQ20051205752). D.G. is supported by Marie Curie Actions (FP7, T3Net).

REFERENCES

Abramoff MD, Magelhaes PJ, Ram SJ (2004). Image processing with ImageJ. Biophotonics Int 11, 36–42.

Carman CV (2009). Mechanisms for transcellular diapedesis: probing and pathfinding by "invadosome-like protrusions." J Cell Sci 122, 3025–3035.

Carman CV, Sage PT, Sciuto TE, de la Fuente MA, Geha RS, Ochs HD, Dvorak HF, Dvorak AM, Springer TA (2007). Transcellular diapedesis is initiated by invasive podosomes. Immunity 26, 784–797.

Collin O, Na S, Chowdhury F, Hong M, Shin ME, Wang F, Wang N (2008). Self-organized podosomes are dynamic mechanosensors. Curr Biol 18, 1288–1294.

Collin O, Tracqui P, Stephanou A, Usson Y, Clement-Lacroix J, Planus E (2006). Spatiotemporal dynamics of actin-rich adhesion microdomains: influence of substrate flexibility. J Cell Sci 119, 1914–1925.

Damljanovic V, Lagerholm B, Jacobson K (2005). Bulk and micropatterned conjugation of extracellular matrix proteins to characterized polyacrylamide substrates for cell mechanotransduction assays. Biotechniques, 39, 847–851.

Destaing O, Block M, Planus E, Albiges-Rizo C (2011). Invadosome regulation by adhesion signaling. Curr Opin Cell Biol 23, 1–10.

Destaing O, Planus E, Bouvard D, Oddou C, Badowski C, Bossy V, Raducanu A, Fourcade B, Albiges-Rizo C, Block MR (2010). β1A integrin is a master regulator of invadosome organization and function. Mol Biol Cell 21, 4108–4119.

Destaing O, Saltel F, Geminard JC, Jurdic P, Bard F (2003). Podosomes display actin turnover and dynamic self-organization in osteoclasts expressing actin-green fluorescent protein. Mol Biol Cell 14, 407–416.

Destaing O, Saltel F, Gilquin B, Chabadel A, Khochbin S, Ory S, Jurdic P (2005). A novel Rho-mDia2-HDAC6 pathway controls podosome patterning through microtubule acetylation in osteoclasts. J Cell Sci 118, 2901–2911.

Geblinger D, Addadi L, Geiger B (2010). Nano-topography sensing by osteoclasts. J Cell Sci 123, 1503–1510.

Hu S, Biben T, Wang X, Jurdic P, Géminard J-C (2011). Internal dynamics of actin structures involved in the cell motility and adhesion: modeling of the podosomes at the molecular level. J Theor Biol 270, 25–30.

Jurdic P, Saltel F, Chabadel A, Destaing O (2006). Podosome and sealing zone: specificity of the osteoclast model. Eur J Cell Biol 85, 195–202.

Linder S (2009). Invadosomes at a glance. J Cell Sci 122, 3009–3013.

Linder S, Aepfelbacher M (2003). Podosomes: adhesion hot-spots of invasive cells. Trends Cell Biol 13, 376–385.

Linder S, Kopp P (2005). Podosomes at a glance. J Cell Sci 118, 2079–2082.

Luxenburg C, Geblinger D, Klein E, Anderson K, Hanein D, Geiger B, Addadi L (2007). The architecture of the adhesive apparatus of cultured osteoclasts: from podosome formation to sealing zone assembly. PLoS One 2, e179.

Riedl J *et al.* (2008). Lifeact: a versatile marker to visualize F-actin. Nat Methods 5, 605–607.

Saltel F, Chabadel A, Bonnelye E, Jurdic P (2008). Actin cytoskeletal organisation in osteoclasts: a model to decipher transmigration and matrix degradation. Eur J Cell Biol 87, 459–468.

Saltel F, Daubon T, Juin A, Ganuza IE, Veillat V, Genot E (2011). Invadosomes: intriguing structures with promise. Eur J Cell Biol 90, 100–107.

Saltel F, Destaing O, Bard F, Eichert D, Jurdic P (2004). Apatite-mediated actin dynamics in resorbing osteoclasts. Mol Biol Cell 15, 5231–5241.

Tsai HH, Macklin WB, Miller RH (2009). Distinct modes of migration position oligodendrocyte precursors for localized cell division in the developing spinal cord. J Neurosci Res 87, 3320–3330.

West MA, Prescott AR, Chan KM, Zhou Z, Rose-John S, Scheller J, Watts C (2008). TLR ligand-induced podosome disassembly in dendritic cells is ADAM17 dependent. J Cell Biol 182, 993–1005.